ISSN 1070-3284, Russian Journal of Coordination Chemistry, 2022, Vol. 48, No. 10, pp. 667–674. © Pleiades Publishing, Ltd., 2022.

A Pair of Chiral Dysprosium Single-Ion Magnets with 2,6-Bis[(4S/4R)4-phenyl-2-oxazolinyl]pyridine and Hexafluoroacetylacetonate Ligands

F. Y. Kong[a], H. Z. Han[a], S. X. Huang[a], Q. H. Teng[a], Y. Li[a], X. Q. Zhang[a], L. Zhu[b, *], K. Wang[a, **], and F. P. Liang[a, *]**

[a] *Guangxi Key Laboratory of Electrochemical and Magnetochemical Functional Materials, College of Chemistry and Bioengineering, Guilin University of Technology, Guilin, 541004 P.R. China*

[b] *School of Chemistry and Materials Engineering, Xinxiang University, Xinxiang, 453003 P.R. China*

**e-mail: zhuli510@xxu.edu.cn*

***e-mail: kaiwang2011@yahoo.com*

****e-mail: fliangoffice@yahoo.com*

Received January 20, 2022; revised April 2, 2022; accepted April 4, 2022

Abstract—Employing 2,6-bis[(4S/4R)-4-phenyl-2-oxazolinyl]pyridine (4R/4S-Pybox) as the chiral inducing ligand, a pair of enantiopure mononuclear Dy(III) complexes, [Dy(Hfac)$_3$(4R/4S-Pybox)] (**1R/1S**; Hfac$^-$ = 1,1,1,5,5,5-hexafluoroacetylacetonate ion) have been synthesized. They are characterized by single-crystal X-ray structure analysis (CCDC nos. 2124459 (**1R**) and 2124460 (**1S**)), elemental analysis, IR spectroscopy, thermogravimetric analysis and powder X-ray diffraction. Within their mononuclear molecular structure, the Dy(III) center locates in a coordination environment afforded by a 4R/4S-Pybox ligand and three Hfac$^-$ ions, displaying a nine-coordinated capped square antiprism coordination geometry with C_{4v} symmetry. Solid circular dichroism spectrum further confirmed their enantiopure nature. Magnetic measurements indicated that **1R** exhibits dual magnetic relaxation behavior, which was rarely observed in chiral SIMs family. The efficient energy barrier and relaxation time for the slow relaxation process are 6.85(4) K and 2.5×10^{-5} s, respectively.

Keywords: Dy(III) complex, chirality, single ion magnet, magnetic properties

DOI: 10.1134/S1070328422100025

INTRODUCTION

During the past few decades, single molecule magnets (SMMs) have attracted great interests owing to their potential applications in high-density data storage, quantum computing, and molecular spintronic devices [1–3]. As the studies moving on, the lanthanide (Ln) ions are increasingly considered to be the idea spin carriers to synthesize high performance SMMs, in particular the Dy(III) ion that possesses a large magnetic moment and Ising-type magnetic anisotropy [4]. A number of Dy-SMMs thus have sprung up in recently years. Strikingly, great progress in performance optimization has been achieved in mononuclear Dy-SMMs, which are also named as the Dy single-ion magnets (Dy-SIMs) [5]. With respect to those of binuclear or polynuclear, these mononuclear systems are easily to synthesized and modified. This facilitates the definition of the types and symmetries of the coordination field of Dy(III) centers, allowing for rational tuning of the single ion anisotropy [6–9]. Several Dy-SIMs with rather high performance have been developed in recently years [10, 11]. More encouragingly, the combination of excellent performance and high stability could be achieved in these systems [12], which further indicate their potential in application.

Endowing the SMMs with additional functions is one of novel topic in their field, as it would helpful for their use as future molecular devices [13, 14]. Particular concerns have been paid to the homochiral SMMs. By introduction of the chirality, other properties could be established in SMMs, such as magneto-optical faraday effects at room temperature [15], third-harmonic generation responses [16], solid-state near-infrared circularly polarized luminescence [17], etc. Even more appealing is that some fantastic synergistic and correlation effects might generate between homochiral structures and inhere magnetic properties. For example, strong interaction between the ferroelectric and magnetic properties has been realized in homochiral {ZnYb} magnets, which afforded amazing room temperature magnetoelectric coupling [18]. Nevertheless, in chiral SMMs family the mononuclear Dy-SIMs were still rare up to now [19–22], despite that they

have showed advantages for high performance. A further exploration of novel chiral Dy-SIMs is thus not only important, but valuable.

Herein we report a pair of Dy-SIMs that formula as (R/S)-[Dy(Pybox)(Hfac)$_3$] (**1R** and **1S**). They were synthesized from the Dy(Hfac)$_3$·2H$_2$O precursor and homochiral Pybox ligand, and show considerable thermostability. Both crystal structural analysis and solid circular dichroism (CD) spectra confirm their enantiomeric nature. Magnetic studies show that the **1R** displays interesting dual magnetic relaxation behavior.

EXPERIMENTAL

Dy(Hfac)$_3$·2H$_2$O was synthesized following previously reported method [23]. Other chemical reagents were purchased from commercial sources and used as received without further purification. The C, H and N microanalyses were carried out with a Model 2400 II, PerkinElmer elemental analyzer. The FT-IR spectra were recorded from KBr pellets in the range 4000–400 cm^{-1} on a PerkinElmer spectrum One FT-IR spectrometer. Thermogravimetric (TG) analyses were performed on a Netzsch STA 449C thermal analyzer from room temperature at a heating rate of 10°C min^{-1} under a continuous stream of N$_2$. Powder X-ray diffraction (PXRD) patterns were recorded using CuK_α radiation on a PANalytical X'Pert PRO diffractometer. The solid CD spectra were recorded at room temperature, using KBr pellets containing a single crystal sample.

All magnetic measurements were performed with polycrystalline samples using a Quantum Design MPMS-3 magnetometer. The variable temperature magnetic susceptibility data were collected over the temperature range of 300~2.0 K, and the isothermal magnetization measurements were carried out between 0 and 7 T. Dynamic (ac) susceptibilities were measured under different external direct current (dc) fields, with an ac field of 2 Oe and frequencies ranging from 1 to 1000 Hz. The experimental magnetic susceptibility data for all samples were corrected for diamagnetic contributions estimated using Pascal's constants and of the sample holder by a previous calibration.

Synthesis of (R)-[Dy(Pybox)(Hfac)$_3$] (1R). A solution of Dy(Hfac)$_3$·2H$_2$O (0.05 mmol, 41 mg) in 25 mL *n*-heptane was refluxed at 95°C and then cooled to 40°C. Then the 4R-Pybox (0.05 mmol, 18.5 mg), 5 mL CH_2Cl_2 and 0.5 mL CH_3OH were added. After being stirred for 30 min, the mixture was cooled to room temperature and filtrated immediately. The filtrate was added with appropriate amount of triethylamine and then left to stand at room temperature for slow evaporation. Colorless block crystals were obtained with the yield of ~58% (based on the Dy(III) salt).

For $C_{38}H_{20}N_3O_8F_{18}Dy$

Anal. calcd., %	C, 39.55	H, 1.91	N, 3.64
Found, %	C, 38.98	H, 1.96	N, 3.53

IR (KBr; ν, cm^{-1}): 3048 s, 1654 s, 1591 w, 1546 w, 1491 s, 1390 s, 1332 w, 1251 w, 1199 w, 1154 w, 1136 s, 970 m, 927 m, 798 m, 744 m, 703 m, 662 s, 584 s.

Synthesis of (S)-[Dy(Pybox)(hfac)$_3$] (1S). A synthetic procedure similar to that of **1R** was used to synthesize **1S**, except that the S-Pybox was used instead of the R-Pybox. The yield was 56% (based on the Dy(III) salt).

For $C_{38}H_{20}N_3O_8F_{18}Dy$

Anal. calcd., %	C, 39.55	H, 1.91	N, 3.64
Found, %	C, 38.94	H, 1.92	N, 3.56

IR (KBr; ν, cm^{-1}): 3050 s, 1662 s, 1589 w, 1504 m, 1487 s, 1384 s, 1259 w, 1207 m, 1154 w, 1142 s, 970 m, 927 m, 796 m, 754 m, 703 w, 672 s, 663 m, 586 s.

X-ray crystallography. All the data were collected with an Agilent SuperNova diffractometer by using graphite monochromatic MoK_α radiation (λ = 0.71073 Å) at 298.15 K. Absorption effect was corrected by semi-empirical methods. The structure was solved by direct methods and was refined by full-matrix least-squares methods with a suite of ShelXS and ShelXL programs via Olex2 interface [24–27]. The non-hydrogen atoms were refined anisotropically. The hydrogen atoms were placed in calculated positions and refined by using a riding model. The final cycle of full-matrix least-squares refinement was based on observed reflections and variable parameters. A summary of crystal data and relevant refinement parameters are given in Table 1.

The full tables of interatomic distances and bond angles, atomic coordinates, and atomic displacement parameters were deposited with the Cambridge Crystallographic Data Centre (CCDC nos. 2124459 (**1R**) and 2124460 (**1S**); deposit@ccdc.cam.ac.uk or https://www.ccdc.cam.ac.uk/structures) and also can be requested from the authors.

RESULTS AND DISCUSSION

The single crystals of **1R** and **1S** were synthesized from Dy(Hfac)$_3$·2H$_2$O and R/S-Pybox ligand in a mixture solvent of *n*-heptane, CH_2Cl_2 and CH_3OH in the presence of minute amount of triethylamine. Synthesis exploration showed that the single crystals could also be obtained without the triethylamine. However, it should be noted that the introduction of triethylamine could promote the quality of single crystals of **1R** and **1S** greatly. It suggests that alkaline synthesis

Table 1. Crystallographic data and refinement parameters for structure of **1R** and **1S**

Parameter	Value	
	1S	**1R**
Empirical formula	$C_{38}H_{22}N_3O_8F_{18}Dy$	$C_{38}H_{22}N_3O_8F_{18}Dy$
Formula weight	1153.08	1153.08
Crystal system	Orthorhombic	Orthorhombic
Space group	$P2_12_12_1$	$P2_12_12_1$
a, Å	12.4017(4)	12.3978(3)
b, Å	18.0075(6)	18.0223(4)
c, Å	19.3115(6)	19.2922(4)
α, deg	90	90
V, Å^3	4312.7(2)	4310.59(2)
Z	4	4
ρ_{calcd}, g/cm^3	1.776	1.777
μ/mm^{-1}	1.864	1.850
F(000)	2252	2252
Reflections collected	36928	34161
Independent reflections	10564	10422
R_{int}	0.0625	0.0361
Data/parameters	10564/613	10422/636
Goodness-of-fit on F^2	1.060	1.050
R_1, wR_2 ($I \geq 2\sigma(I)$)	0.0443, 0.0735	0.0345, 0.0649
R_1, wR_2 (all data)	0.0797, 0.0901	0.0477, 0.0718
Flack parameter	−0.026(1)	−0.034(5)

condition may be in favor of the formation of single crystals of **1R** and **1S**.

Single crystal X-ray diffraction analysis revealed that **1R** and **1S** crystalliz in chiral $P2_12_12_1$ space groups. As shown in Fig. 1a, each complex consists of a Dy(III) ion, a R- or S-Pybox ligand and three $Hfac^-$ ion. The Dy(III) ion locates in a coordination environment afforded by six O atoms of $Hfac^-$ and three N atoms from Pybox ligand, forming a nine-coordinated spherical capped square antiprism coordination configuration with C_{4v} symmetry (Fig. 1b) as suggested by continuous shape measurement (CShM) using SHAPE 2.0 software (Table 2) [28, 29]. The Dy−O and Dy−N bond lengths range from 2.346(5)−2.441(6) and 2.558(6)−2.593(7) Å, respectively. No matter from whole molecule structures or coordination geometries of the Dy(III) ions, the **1R** and **1S** present mirror symmetry, indicating their enantiopure nature. In crystal lattice the molecules stack in relative sparse way. Intermolecular the shortest Dy···Dy distances for **1R** and **1S** are 9.348 and 9.340 Å (Fig. 2), representing intermolecular interaction can be negligible.

The TG curves of **1R** and **1S** were measured in the temperature range of 35−800°C with a heating rate of 10°C/min in a N_2 atmosphere. Two complexes showed rather similar TG behavior (Fig. 3). Upon heating, their samples keep stable until about 220°C, after which the decomposition started to happen. These results indicated that both **1R** and **1S** possess considerable thermal stability. On the other hand, the PXRD of **1R** and **1S** were measured with crystalline powder samples at room temperature. The experimental curves for both complexes were in good agreement with their simulated patterns (Fig. 4), respectively, demonstrating their phase purity.

The homochirality of **1R** and **1S** were further checked by solid CD spectra. As shown in Fig. 5, the CD spectra of **1R** and **1S** display obvious mirror symmetry effect. The CD spectra of **1S** exhibits a strong negative Cotton effect near 353 nm, and **1R** appear as positive Cotton effect at the same wavelengths. These results are indicative of the homochirality of them. They also signify that **1R** and **1S** are pair of enantiomers.

Considering the enantiomeric nature of **1R** and **1S**, the **1R** was selected as the representative to investigate

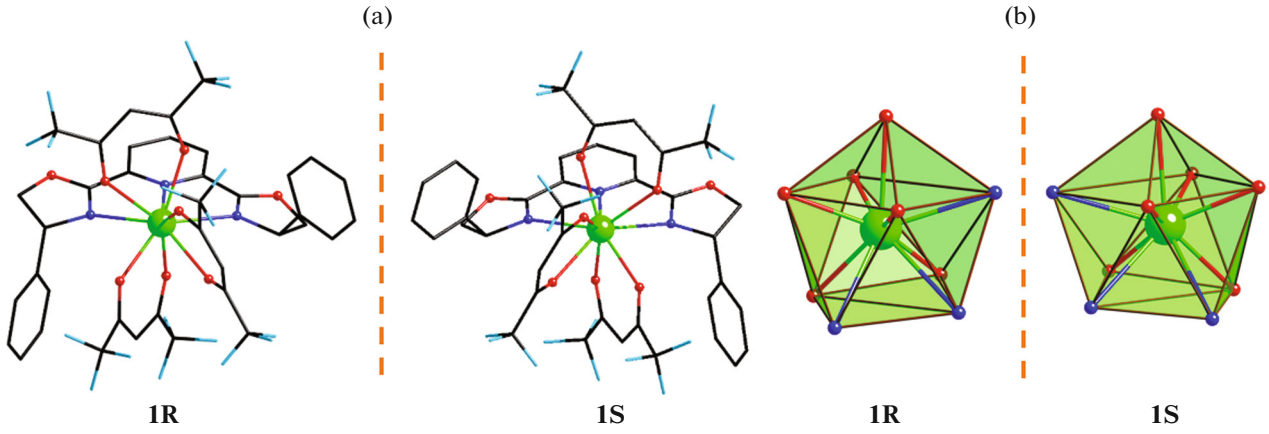

Fig. 1. Crystal structures (a) and the coordination geometries of the Dy(III) centers (b) of **1R** and **1S**.

their magnetic properties. The direct current (dc) magnetic susceptibility of **1R** was measured in the temperature range of 300–2.0 K under an external dc magnetic field of 1.0 kOe. As shown in Fig. 6, the $\chi_M T$–T curve of **1R** presents an obvious temperature dependent tendency. At room temperature the $\chi_M T$ value is 14.78 cm^3 K mol^{-1}, which is close to the theoretical value of 14.17 cm^3 K mol^{-1} for a magnetic isolated Dy(III) ion ($S = 5/2$, $L = 5$, $g = 4/3$, and $^6H_{15/2}$). As the temperature decreasing, the $\chi_M T$ value decreases gradually until about 20 K. Then the value decreases rapidly and finally reaches to the minimum of 9.27 cm^3 K mol^{-1} at 2 K. This behavior might be caused by the progressive quenching of Stark sublevel of the Dy(III) ion [30].

The variable field magnetization of **1R** was recorded at 2, 2.5, 5 and 10 K. As shown in Fig. 7, the M values at different temperature all increase with the increasing of external field. The M value at 2 K and 7 T is 6.98 $N\mu_B$, being lower than the expected theoretical values of 10 $N\mu_B$ for one Dy(III) ion. The non-superposition of the M–H curves suggests the presence of significant magnetic anisotropy and/or low-lying excited states of the Dy(III) ion in **1R** [31, 32].

In order to investigate the dynamic magnetic behaviors of **1R**, alternating current (ac) magnetic susceptibility measurements were first performed under different applied dc field in a frequency range of 1–1000 Hz at 2 K (Fig. 8). None of the in-phase (χ') and out-phase (χ") signals could be observed under zero field. As the increasing of the dc fields, the χ" signals started to appear and became much pronounced. It is the indicative of successful suppression of quantum tunneling magnetization (QTM) process by applied dc field. Meanwhile, the high-frequency peaks declined gradually, and new peaks in low-frequency range emerged and reached to the maximum at 2.0 kOe. This suggests a dual magnetic relaxation behavior [33, 34]. On this basis, the applied dc field of 2.0 kOe was selected to further investigate the dynamic magnetic properties of **1R**.

When a 2.0 kOe dc field was applied, the χ" signals show obvious dual relaxation including both fast and slow relaxation processes (FR and SR) at low temperature (Fig. 9). The data was fitted to the sum of two

Table 2. The calculated results for Dy(III) ions configuration for **1R** and **1S**

Configuration	Symmetry	**1R**	**1S**
Enneagon	D_{9h}	35.066	35.003
Octagonal pyramid	C_{8v}	22.564	22.612
Heptagonal bipyramid	D_{7h}	17.615	17.606
Johnson triangular cupola J3	C_{3v}	15.842	15.857
Capped cube J8	C_{4v}	10.717	10.704
Spherical-relaxed capped cube	C_{4v}	9.589	9.557
Capped square antiprism J10	C_{4v}	2.115	2.107
Spherical capped square antiprism	C_{4v}	**1.101**	**1.073**
Tricapped trigonal prism J51	D_{3h}	3.711	3.715

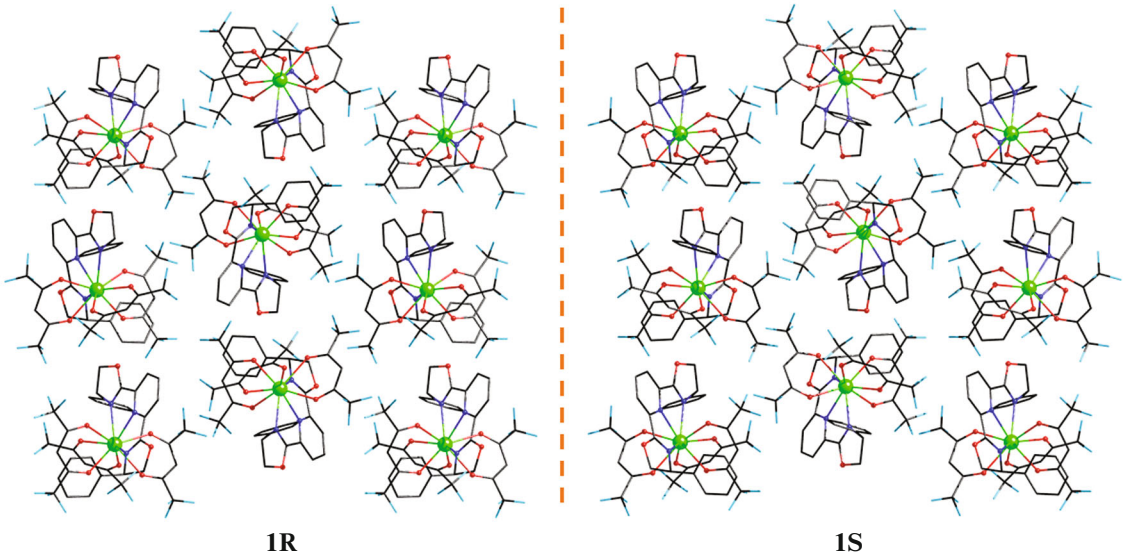

Fig. 2. Packing diagrams of **1R** and **1S** viewed from *a*-axis direction.

modified Debye functions [35], which gave Cole–Cole plots where the curves displayed asymmetric double semicircles in low temperature range

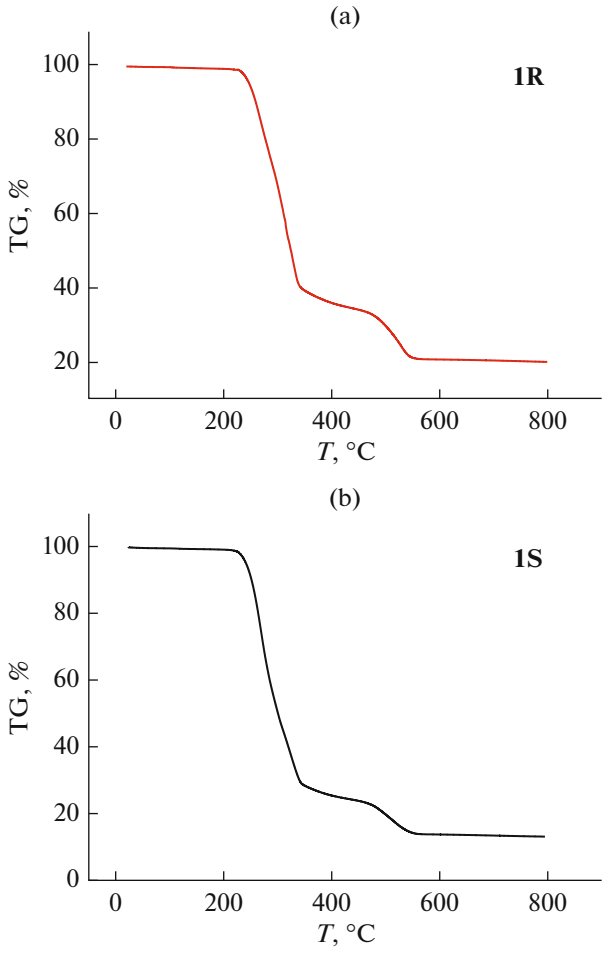

Fig. 3. TG curves of **1R** and **1S**.

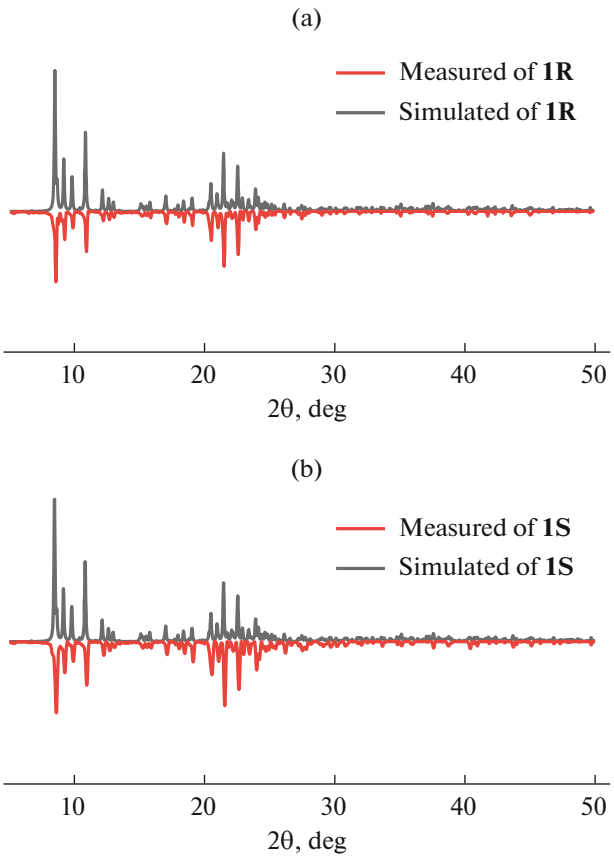

Fig. 4. PXRD patterns of **1R** and **1S**.

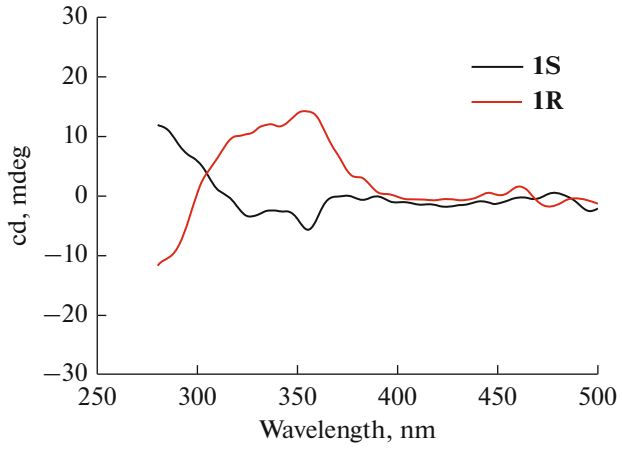

Fig. 5. Solid CD spectra of **1R** and **1S** at room temperature.

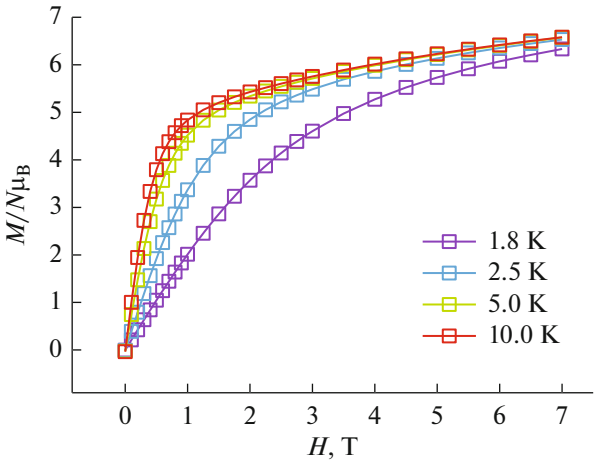

Fig. 7. Plots of M versus H of **1R**.

(Fig. 10a). As the signals of FR were too weak, only the data of SR was fitted (Fig. 10b). Corresponding fitting based on $\ln(\chi''/\chi') = \ln(\omega\tau_0) + U_{eff}/k_BT$ [36], give the efficient energy barrier (U_{eff}) and relaxation time (τ_0) of 6.85(4) K and 2.5×10^{-5} s, respectively.

In previous literature, few Dy-SIMs whose Dy centers show capped square-antiprism geometry have been reported. Limited cases include $[Dy(Tpz)_2Bpz]\cdot 0.5CH_2Cl_2$ [Tpz = hydrotris(pyrazolyl)-borate; Bpz = dihydrobis(pyrazolyl)borate] [37], $[Dy(H_3L)(OAc)](ClO_4)_2\cdot MeOH\cdot H_2O$ [H_3L = tris[2-(((imidazol-4-yl)methylidene)amino)-ethyl]amine] [38], and $[Dy(HL_3)_3(NO_3)_3]\cdot CH_3CN$ (HL_3 = (1-[N-(4-methoxyl) aminomethylidene-2(1H)-naphthalenone) [39]. The **1R** are comparable to these reported cases in the aspect of performance parameters. However, within the magnetic relaxation of these mononuclear capped square-antiprismatic Dy systems, there exist phonon-assisted tunneling process with a dominant contribution from the first excited doublet [38]. It weakened U_{eff} of these systems to some extent.

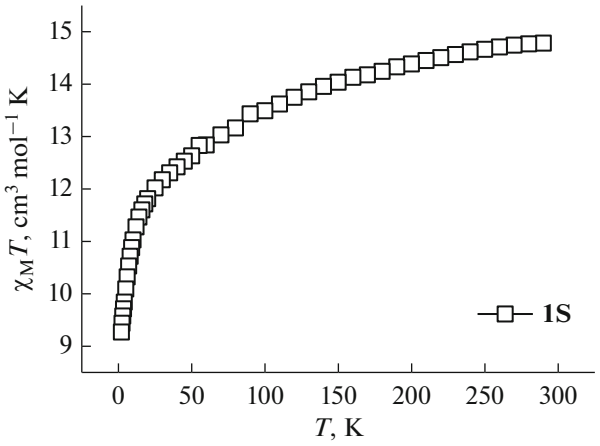

Fig. 6. Plots of $\chi_m T$ versus T of **1R**.

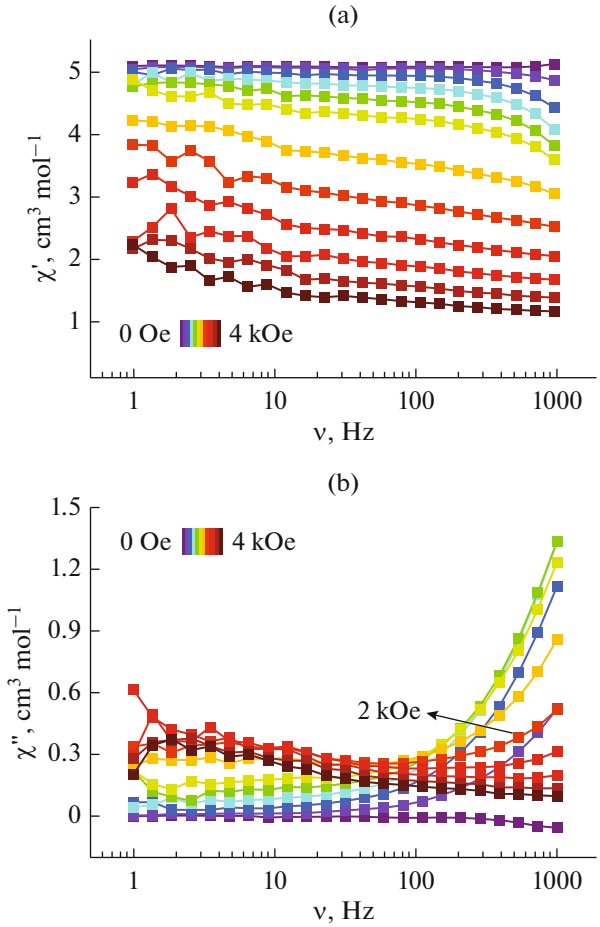

Fig. 8. Frequency-dependent χ' (a) and χ'' (b) signals of **1R** at 2 K and under different dc fields.

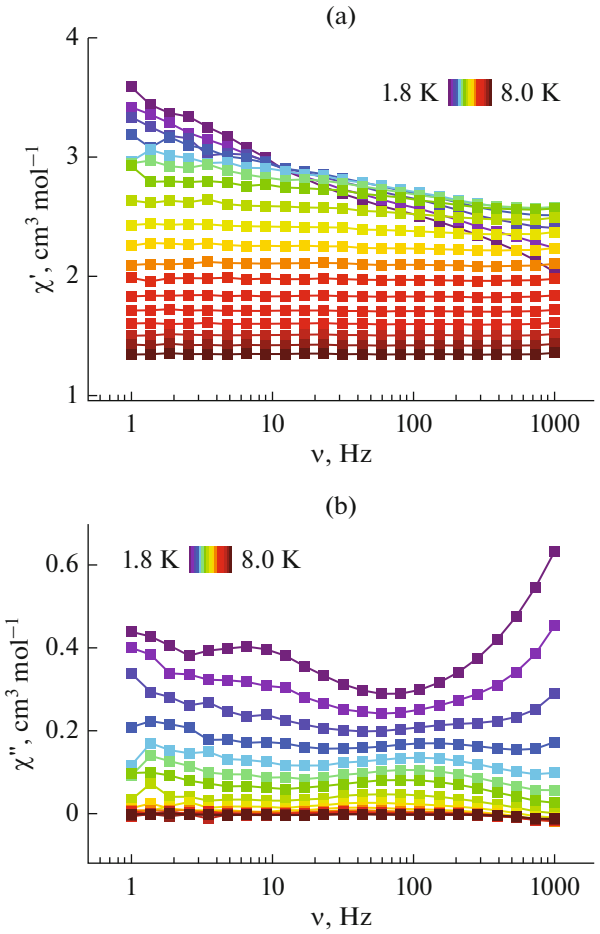

Fig. 9. Frequency-dependent χ' (a) and χ" (b) signals of **1R** at 1.8–8 K and under 2.0 kOe applied fields.

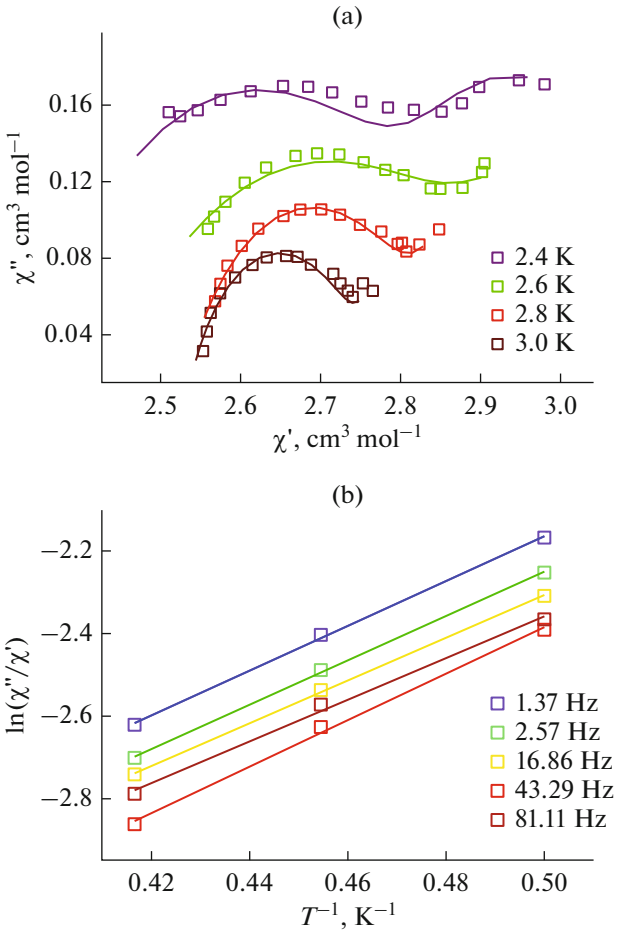

Fig. 10. Cole–Cole (a) and $\ln(\chi''/\chi')-T^{-1}$ plot (b) of **1R**.

In conclusion, a pair of chiral Dy-SIMs (**1R** and **1S**) were synthesized using chiral Pybox ligand. Crystal structure analysis and solid CD spectrum established their enantiopure nature. Magnetic studies indicated that **1R** exhibited field-induced dual relaxation behavior containing both FR and SR processes. More importantly, both **1R** and **1S** keep stable until about 220°C. In present family of Dy-SIMs, the chiral species were still limited, and the stable chiral cases were particularly scarcity. The present work thus affords rare Dy-SIMs featuring both homochirality and good thermal stability. A further exploration of other properties in addition to their SMM behavior is in progress.

FUNDING

This work was financially supported by the National Natural Science Foundation of China (grants nos. 21961008 and 22075058).

CONFLICT OF INTEREST

The authors declare that they have no conflicts of interest.

AUTHOR CONTRIBUTIONS

F.Y. Kong and H.Z. Han have contributed equally to this work.

REFERENCES

1. Sessoli, R., Gatteschi, D., Caneschi, A., et al., *Nature*, 1993, vol. 365, p. 141.
2. Zhang, P., Guo, Y.N., and Tang, J.K., *Coord. Chem. Rev.*, 2013, vol. 257, p. 1728.
3. Sessoli, R. and Powell, A.K., *Coord. Chem. Rev.*, 2009, vol. 253, p. 2328.
4. Liddle, S.T. and Slageren, J.V., *Chem. Soc. Rev.*, 2015, vol. 44, p. 6655.
5. Liu, J.L., Chen, Y.C., and Tong, M.L., *Chem. Soc. Rev.*, 2018, vol. 47, p. 2431.
6. Goodwin, C.A.P., Ortu, F., Reta, D., et al., *Nature*, 2017, vol. 548, p. 439.

7. Guo, F.S., Day, B.M., Chen, Y.C., et al., *Science*, 2018, vol. 362, p. 1400.
8. Chen, Y.C., Liu, J.L., Ungur, L., et al., *J. Am. Chem. Soc.*, 2016, vol. 138, p. 28290.
9. Harriman, K.L.M., Brosmer, J.L., Ungur, L., et al., *J. Am. Chem. Soc.*, 2017, vol. 139, p. 1420.
10. Goodwin, C.A.P., Ortu, F., Reta, D., et al., *Nature*, 2017, vol. 548, p. 439.
11. Guo, F.S., Day, B.M., Chen, Y.C., et al., *Angew. Chem. Int. Ed.*, 2017, vol. 56, p. 11445.
12. Zhu, Z.H., Zhao, C., Feng, T.T., et al., *J. Am. Chem. Soc.*, 2021, vol. 143, p. 10077.
13. Feng, M., Ruan, Z.Y., Chen, Y.C., et al., *Chem. Commun.*, 2020, vol. 56, p. 13702.
14. Cador, O., Guennic, B.L., and Pointillart, F., *Inorg. Chem. Front.*, 2019, vol. 6, p. 3398.
15. Liu, C.M., Sun, R., Wang, B.W., et al., *Inorg. Chem.*, 2021, vol. 60, p. 12039.
16. Cui, M.H., Yang, L.P., Li, F.C., et al., *Inorg. Chem.*, 2021, vol. 60, p. 13366.
17. Lefeuvre, B., Mattei, C.A., Gonzalez, J.F., et al., *Chem. Eur. J.*, 2021, vol. 27, p. 7362.
18. Long, J., Ivanov, M.S., Khomchenko, V., et al., *Science*, 2020, vol. 367, p. 671.
19. Zhu, Z.H., Zhao, C., Feng, T.T., et al., *J. Am. Chem. Soc.*, 2021, vol. 143, p. 10077.
20. Li, D.P., Wang, T.W., Li, C.H., et al., *Chem. Commun.*, 2010, vol. 46, p. 2929.
21. Li, X.L., Chen, C.L., Gao, Y.L., et al., *Chem. Eur. J.*, 2012, vol. 18, p. 14632.
22. Chen, Y.X., Ma, F., Zhang, Y.H., et al., *Inorg. Chem. Front.*, 2018, vol. 5, p. 2006.
23. Pointillart, F., Bernot, K., Sessoli, R., et al., *Inorg. Chem.*, 2010, vol. 49, p. 4355.
24. Sheldrick, G.M., *SHELX-2014, Programs for Crystal Structure Analysis,* Göttingen: Univ. of Göttingen, 2014.
25. Sheldrick, G.M., *Acta Crystallogr., Sect. C: Struct. Chem.*, 2015, vol. 71, p. 3.
26. Dolomanov, O.V., Bourhis, L.J., Gildea, R.J., et al., *J. Appl. Crystallogr.*, 2009, vol. 42, p. 339.
27. Bourhis, L.J., Dolomanov, O.V., Gildea, R.J., et al., *Acta Crystallogr., Sect A: Found. Adv.*, 2015, vol. 71, p. 59.
28. Zabrodsky, H., Peleg, S., and Avnir, D., *J. Am. Chem. Soc.*, 1992, vol. 114, p. 7843.
29. Pinsky, M. and Avnir, D., *Inorg. Chem.*, 1998, vol. 37, p. 5575.
30. Ling, B.K., Zhai, Y.Q., Han, J., et al., *Dalton Trans.*, 2020, vol. 49, p. 6969.
31. Liu, S.S., Meng, Y.S., Zhang, Y.Q., et al., *Inorg. Chem.*, 2017, vol. 56, p. 7320.
32. Kalita, P., Ahmed, N., Bar, A.K., et al., *Inorg. Chem.*, 2020, vol. 59, p. 6603.
33. Lin, C.B., Guo, K.K., Guo, W.X., et al., *Inorg. Chem.*, 2020, vol. 59, p. 16924.
34. Su, S.D., Li, J.X., Xu, F., et al., *Dalton Trans.*, 2020, vol. 49, p. 15739.
35. Guo, Y.N., Xu, G.F., Guo, Y., et al., *Dalton Trans.*, 2011, vol. 40, p. 9953.
36. Bartolomé, J., Filoti, G., Kuncser, V., et al., *Phys. Rev. B*, 2009, vol. 80, p. 014430.
37. Lannes, A. and Luneau, D., *Inorg. Chem.*, 2015, vol. 54, p. 6736.
38. Shintoyo, S., Murakami, K., Fujinami, T., et al., *Inorg. Chem.*, 2014, vol. 53, p. 10359.
39. Yang, H., Liu, S.S., Meng, Y.S., et al., *Dalton Trans.*, 2022, vol. 51, p. 1415.